

1 **Phylogenetic Tree-based Pipeline for Uncovering Mutational** 2 **Patterns during Influenza Virus Evolution**

3
4 Fransiskus Xaverius Ivan¹, Akhila Deshpande¹, Chun Wei Lim¹, Xinrui Zhou¹, Jie Zheng², Chee
5 Keong Kwoh¹

6
7 ¹ Biomedical Informatics Lab, School of Computer Science and Engineering, Nanyang
8 Technological University, Singapore

9 ² School of Information Science and Technology, ShanghaiTech University

10

11 *Corresponding author: fivan@ntu.edu.sg

12

13 **Abstract**

14

15 Various computational and statistical approaches have been proposed to uncover the mutational
16 patterns of rapidly evolving influenza viral genes. Nonetheless, the approaches mainly rely on
17 sequence alignments which could potentially lead to spurious mutations obtained by comparing
18 sequences from different clades that coexist during particular periods of time. To address this issue,
19 we propose a phylogenetic tree-based pipeline that takes into account the evolutionary structure in
20 the sequence data. Assuming that the sequences evolve progressively under a strict molecular
21 clock, considering a competitive model that is based on a certain Markov model, and using a
22 resampling approach to obtain robust estimates, we could capture statistically significant single-
23 mutations and co-mutations during the sequence evolution. Moreover, by considering the results
24 obtained from analyses that consider all paths and the longest path in the resampled trees, we can
25 categorize the mutational sites and suggest their relevance. Here we applied the pipeline to
26 investigate the 50 years of evolution of the HA sequences of influenza A/H3N2 viruses. In addition
27 to confirming previous knowledge on the A/H3N2 HA evolution, we also demonstrate the use of
28 the pipeline to classify mutational sites according to whether they are able to enhance antigenic
29 drift, compensate other mutations that enhance antigenic drift, or both.

30 Introduction

31

32 Seasonal influenza viruses, especially the influenza A viruses, have exhibited frequent mutations
33 with a rapid evolutionary rate. The hemagglutinin (HA) of influenza has the highest mutational
34 rate among all influenza viral proteins [1]. Besides, the HA is considered as a major culprit for the
35 antigenicity of influenza and a primary target for the influenza vaccine [2, 3]. Cumulative
36 mutations can lead to the antigenic drift of influenza, enable the viruses to mismatch the influenza
37 vaccine, escape the human immune system, and even raise an epidemic [4]. Therefore, it is crucial
38 to surveil and predict the mutations of influenza. The knowledge of mutational patterns can
39 improve our understanding about the mechanism of antigenic drift.

40

41 Discovering the dependencies among mutations is a non-trivial and active area of bioinformatics.
42 Non-independent mutations of amino acids may co-occur, or occur chronologically, generally
43 sharing a common constraint or protein function domain [5]. The directed mutagenesis
44 experiments are a classical type of method to identify functional dependencies between amino acid
45 sites [6]. However, the complexity of possible the experiments limits the capacity of research.
46 Subsequently, various statistical and computational models have been proposed as complementary
47 tools to evaluate the correlation between amino acid sites [7], annotate protein functional domains
48 [8], reveal possible amino acid interactions, and predict the interactions between motifs or proteins
49 [9, 10].

50

51 As to the influenza viruses, many computational methods detecting the antigenic mutations have
52 been proposed. For example, Smith *et al.* pioneered the mapping of antigenic evolution and genetic
53 evolution, revealing that the influenza viruses undergo continuous genetic evolution pressure,
54 while the antigenic evolution is more punctuated with 11 antigenic clusters of influenza A/H3N2
55 being detected. The comparison between genetic and antigenic evolution indicated that some
56 mutations bear a disproportionately large effect on the antigenicity of influenza [11]. Shih *et al.*
57 analyzed the frequency changes of all HA1 amino acids, showing that the positive selection on
58 HA1 is ongoing most of the time. However, the antigenic drift of influenza is punctuated which
59 can be changed by a single substitution at antigenic sites of HA1, or in most cases, by simultaneous
60 multiple fixations [12]. Koel *et al.* extended the works by investigating the antigenic clusters and

61 all observed substitutions. It was found that seven cluster-transition substitutions were responsible
62 for the antigenic cluster transitions, all of which located at or around the receptor-binding sites of
63 HA [13]. Recently, Quan *et al.* developed a computational model RECDS (recognition of cluster-
64 transition determining sites) using a gradient boosting classifier to rank the importance of all HA
65 sites, and evaluate the contribution of an HA amino acid site to the antigenic evolutionary history
66 of influenza viruses [14]. The RECDS is a feature-based (both sequence-based features and
67 structure-based features) computational model under the assumption that features dominating
68 antigenicity are highly conserved. Statistical models on positive selection sites are mainly based
69 on the ratio of nonsynonymous to synonymous mutations (dN/dS ratio) [15]. Tusche *et al.*
70 integrated the dN/dS as a measure of selection, the ancestral information inferred from
71 phylogenetic trees, and spatial proximity of sites to identify regions under selective pressure [16].
72

73 However, these methods do not pay attention to the substitution dependency on the HA.
74 Information theory based strategies are the most extensively used to measure the covariance
75 between mutations [17]. For example, Baker *et al.* developed a web-based tool CoeViz for
76 calculating and visualizing covariance metrics (mutual information, chi-square statistics, Pearson
77 correlation, and joint Shannon entropy) [18]. Xia *et al.* constructed a site transition network based
78 on the pairwise mutual information between amino acids of the HA sequences [19]. The network
79 incorporating correlation information between residues improved the prediction of site mutations
80 with an accuracy of 70%. Besides, Elma *et al.* considered the information of HA evolution. A
81 mass-based protein phylogenetic model was proposed to identify functional mutations [20].
82 Alternatively, machine learning approaches are also applied to detect mutation patterns. For
83 example, Chen *et al.* applied association rule mining to explore co-occurring mutations on H3 [21].
84 Du *et al.* proposed a feature-based Naïve Bayesian network to predict antigenic clusters [22].
85

86 However, those methods mainly depend on the protein sequences, lacking the chronological and
87 3D structural information. In this study, we proposed a pipeline for uncovering not only single-
88 mutations under positive selection pressure, but also co-mutations of influenza viral protein
89 sequences. Besides, we analyzed the co-mutations of hemagglutinin sequences of human influenza
90 A/H3N2 to evaluate the effectiveness and robustness of the proposed pipeline. The detected
91 mutation sites are highly overlapped with those reported to be under positive selection pressure,

92 especially interfaces exposed to the antigenic binding. The proposed pipeline is promising to be
93 applied to analyzing the molecular evolution of all influenza proteins.

94

95 **Methods**

96

97 The flowchart of the proposed pipeline for uncovering significant single-mutations and co-
98 mutations in particular influenza protein sequences is presented in **Fig. 1**. The overall pipeline
99 composed of five major procedures, i.e., (i) Sub-pipeline 1 that retrieved, clustered and aligned a
100 subset of sequence data from local influenza genome datasets, (ii) Sub-pipeline 2 that identified
101 and removed outliers detected following the linear regression of root-to-tip distances in inferred
102 neighbor joining (NJ) tree against isolation dates, (iii) Sub-pipeline 3 that extracted substitution
103 model parameters from a maximum likelihood (ML) tree reconstructed from aligned sequences
104 and used them to simulate sequence evolution, (iv) Sub-pipeline 4 that reconstructed resampled
105 trees from aligned sequence data (either real or simulated one), and (v) Sub-pipeline 5 that
106 calculated supports for single-mutations and co-mutations detected in the resampled trees. The
107 evolutionary parameters, i.e., the rate of substitution and the date of origin, were required for co-
108 mutation detection and remaining analyses (interpretation), and could be robustly estimated from
109 the root-to-tip regressions of the resampled trees. At the final stage, the distributions of supports
110 for the single-mutations/co-mutations from simulated sequence data were used to set a threshold
111 for claiming significant single-mutations/co-mutations from the real sequence data. The details of
112 the local influenza genome datasets and steps in each major procedure in the pipeline are described
113 shortly, while the use of the pipeline for analyzing the evolutionary patterns of the hemagglutinin
114 (HA) sequences of human influenza A/H3N2 viruses are presented in the Results and Discussions.

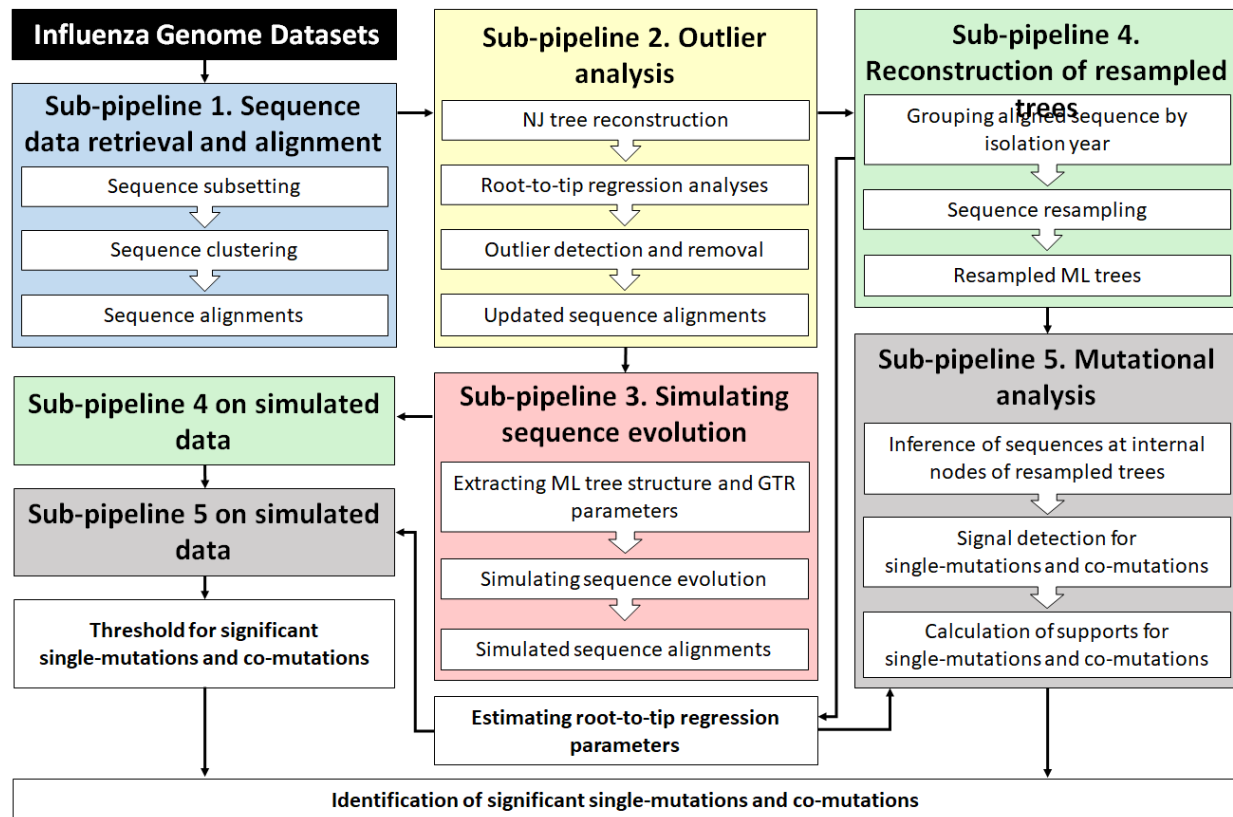
115

116 **Influenza genome datasets.** Local datasets consisting of influenza virus genomes, transcriptomes,
117 proteomes, and their metadata (including the virus types, virus subtypes, virus names, and date of
118 isolation) were created for this work. The records were retrieved from NCBI Influenza Virus
119 Resource [23] or GISAID database [24]. Only records of influenza viruses whose genome was
120 complete, associated coding/protein sequences could be identified and were not too short, and
121 information of the host, location, and date of collection (for the date, if only the day was missing,
122 then it was set to the 15th of the month; if the day and the month were missing, then it was set to

123 30 June of the year) was available, were included in the datasets. The records were cleaned and
 124 reformatted into one tab-delimited text file of metadata and eight tab-delimited text files of
 125 sequence data that correspond to each of the eight segments of influenza virus genome.

126

127 **Fig. 1.** Phylogenetic tree-based pipelines for uncovering significant single-mutations and co-
 128 mutations in evolving influenza viral proteins.



129

130

131 **Sub-pipeline 1 – Sequence data retrieval and alignment.** This pipeline was used to subset the
 132 full nucleotide sequences, coding sequences and protein sequences of a particular gene of a specific
 133 influenza A subtype or influenza B lineage from the local datasets described previously, and each
 134 of the dataset was stored into a fasta file. The description of each fasta sequence record included
 135 the sequence ID, gene name, genome ID, name of the corresponding influenza virus strain, country
 136 and the date of virus isolation. The subsetted, non-redundant coding sequences were then aligned
 137 to codon position. For fast alignment and considering the sequences were highly similar, the
 138 protein sequences were first clustered using the CD-HIT tool [25] to obtain clusters of sequences
 139 whose percent identity to a representative sequence was above a certain threshold (we used a

140 threshold of 98%). Clusters containing protein sequences of different length were split according
141 to their length. Subsequently, the representatives of CD-HIT clusters were aligned with the muscle
142 package [26] and the protein alignment was then used to guide the alignment of the corresponding
143 coding sequences to codon position. The alignment of each of the rest of the coding sequences to
144 the alignment of the representatives was done according to the alignment of its corresponding
145 representative. The results of the alignment were visualized with MEGA7 software [27] for
146 inspection.

147
148 **Sub-pipeline 2 – Outlier analysis.** For outlier detection, we assumed that the sequence evolution
149 follows a strict molecular clock, i.e., all branches in the phylogenetic tree evolve at the same rate.
150 To evaluate this assumption, the genetic distances based on Jukes-Cantor (JC) substitution model
151 [28] were calculated from the aligned coding sequences and used to construct an NJ tree [29].
152 Assuming the sequences evolve progressively, the phylogenetic tree was rooted using one of the
153 earliest coding sequence as an outgroup. The root-to-tip regression analysis was then used to
154 explore the association between genetic distances of the samples from the tree root and sampling
155 dates. Denoting these two variables as $d_{r,i}$ and t_i , respectively, where r represents the tree root
156 and i represents the samples or tree tips, the regression model can be written as: $E[d_{r,i}] =$
157 $\mu(t_i - t_r)$. The gradient (μ) and x -intercept (t_r) provide estimates for the substitution rate and the
158 time of the tree root (the date of origin), respectively. Given the nature of the sequence data that is
159 heterochronous (collected at different time points), a strong linear correlation between $d_{r,i}$ and t_i
160 suggests a high level of strict clock-like signals. Due to the non-independency of the individual
161 data points, the root-to-tip linear regression is not appropriate for statistical hypothesis [30].
162 Nonetheless, the regression approach is reasonably used for identifying outliers. Here we identified
163 a data point as an outlier if the absolute value of its residual from the regression line was larger
164 than five times interquartile range.

165
166 **Sub-pipeline 3 – Simulating sequence evolution.** After outliers were removed, a new
167 phylogenetic tree was reconstructed using a more complex substitution model and algorithm. In
168 particular, we reconstructed an ML tree using $GTR + G + I$ substitution model implemented in
169 phangorn package [31]. The GTR substitution model [32] is a type of continuous-time Markov
170 model that is most general neutral, independent, finite-sites and time-reversible model. Its

171 parameters consist of four equilibrium base frequency parameters (π_A : the frequency of base A,
 172 π_G : the frequency of base G, π_C : the frequency of base C, and π_T : the frequency of base T) and
 173 six substitution rate parameters (α : the substitution rate parameter for A \rightarrow G and G \rightarrow A, β : the
 174 substitution rate parameter for A \rightarrow C and C \rightarrow A, γ : the substitution rate parameter for A \rightarrow T
 175 and T \rightarrow A, δ : the substitution rate parameter for G \rightarrow C and C \rightarrow G, ε : the substitution rate
 176 parameter for G \rightarrow T and T \rightarrow G, and η : the substitution rate parameter for C \rightarrow T and T \rightarrow C).
 177 These parameters form the equilibrium base frequency vector $\Pi = (\pi_A, \pi_G, \pi_C, \pi_T)$ and the rate
 178 matrix

$$179 \quad Q = \begin{bmatrix} -(\alpha\pi_G + \beta\pi_C + \gamma\pi_T) & \alpha\pi_G & \beta\pi_C & \gamma\pi_T \\ \alpha\pi_A & -(\alpha\pi_A + \delta\pi_C + \varepsilon\pi_T) & \delta\pi_C & \varepsilon\pi_T \\ \beta\pi_A & \delta\pi_G & -(\beta\pi_A + \delta\pi_G + \eta\pi_T) & \eta\pi_T \\ \gamma\pi_A & \varepsilon\pi_G & \eta\pi_C & -(\gamma\pi_A + \varepsilon\pi_G + \eta\pi_C) \end{bmatrix}$$

180 for the continuous-time Markov model. When considering the *GTR + G + I* model, a discrete
 181 Gamma distribution (+*G*) is used to take into account the rate heterogeneity among sites and a
 182 fixed fraction of sites is assumed to be evolutionary invariable (+*I*). These add two parameters for
 183 the Gamma distribution, i.e., the number of rate categories and the shape parameters, and another
 184 parameter for the proportion of invariant sites into the model. The estimated *GTR + G + I*
 185 substitution model parameters, the structure of the ML tree (that included the length of their
 186 branches) and the sequence at the tree root (inferred using Fitch algorithm [33]), were then used
 187 to simulate sequence evolution with Pyvolve [34]. Note that Pyvolve does not model
 188 insertion/deletion, hence any gap in the root sequence were removed. Sequences produced at the
 189 tip of the tree as the results of simulation were used to create a new sequence dataset that is referred
 190 to as simulated sequence dataset.

191
 192 **Sub-pipeline 4 – Reconstruction of resampled trees.** To reconstruct resampled phylogenetic
 193 trees from real or simulated sequence dataset, the aligned sequences were first grouped according
 194 to their sampling year. Before grouping, one of the earliest sequence was first singled out and it
 195 will always be included for sampled tree reconstruction. The grouping was done year by year, i.e.,
 196 starting from the earliest year to the latest year, and the earlier sequences were grouped into a
 197 single year group if the total number of the sequences was more than a certain threshold (here we
 198 used a threshold of 20). After sequence grouping, we repeatedly and randomly sampled a fixed
 199 number of aligned sequences from each year group and added the earliest sequence to the sample.

200 An ML phylogenetic tree was then reconstructed for each sample using a $GTR + G + I$ substitution
201 model implemented in phangorn package. The resampled ML trees were rooted using the earliest
202 sequence as an outgroup and then used to calculate bootstrap estimates for the substitution rate and
203 the date of sequence origin, i.e., by averaging the estimates obtained from each tree using the root-
204 to-tip regression approach.

205

206 **Sub-pipeline 5 – Mutational analysis with resampled trees.** Mutational analysis was done using
207 resampled phylogenetic trees from each of the real and simulated sequence data. Each edge length
208 or distance between two adjacent nodes in the trees was associated with the evolutionary distance,
209 i.e., the number of nucleotide substitutions per site estimated based on the chosen substitution
210 model. The distance between any two nodes (of interest, between ancestor and predecessor) in the
211 tree was calculated by summing the length of edges in the path connecting the two nodes. The
212 coding and protein sequences at each internal node of each tree were inferred using the Fitch's
213 algorithm [33]. Amino acid mutations were detected at each node (except for the root) by
214 comparing its protein sequence to its parent's protein sequence. Each amino acid mutation was in
215 the form AA1- p -AA2, representing a mutation of a given amino acid AA1 in the parent node to
216 another amino acid AA2 in the child node at a given site p in the sequence. Finally, the distance
217 of each node to the root of the tree was also recorded.

218

219 The resampled phylogenetic trees were used to calculate support values that indicate the signal
220 strength of single-mutational and co-mutational events during sequence evolution. To calculate
221 supports for single-mutations, each of single-mutations observed in the trees was mapped to a list
222 of real numbers representing the distances of the nodes where the mutation observed to their
223 corresponding root. Then, for each mutation, we smoothed the distribution of its distance data with
224 a Gaussian kernel density estimate [35], followed by the detection of the peaks that were defined
225 as local maxima centered in any interval for the distance. Assuming h_1, h_2, \dots, h_k are the heights
226 of the detected peaks for mutation m at distance to the root d_1, d_2, \dots, d_k , then the strength of the
227 signal for m at distance d_i , denoted by $S(m, d_i)$, was calculated as follows: $S(m, d_i) =$
228 $h_i N / \sum_{j=1}^{j=m} h_j$, where N is the number of observations for the mutation of interest. The formula is
229 indicative of the portion of observations that support the observed mutation. In addition to
230 calculating supports for single-mutations found in any node in the resampled trees, we also

231 calculated supports for single-mutations that were only observed in the longest paths of the
232 resampled trees. The version of mutational analysis that considers any path in the resampled trees
233 is termed as all path analysis, while the one that considers the longest path is termed as the longest
234 path analysis.

235
236 The supports for co-mutations were calculated in similar way. Here, we considered co-mutations
237 as any possible pair of single-mutations (the order of the single-mutations does not matter)
238 observed at a single node or from two different nodes that had ancestor-predecessor relationship
239 and distance below a certain threshold (which ought to be influenced by the estimated substitution
240 rate). Each co-mutation was mapped to the distance of the ancestral node to the root of its
241 resampled tree. Note that if the co-mutation was observed at a single node, then the node was
242 considered as both ancestor and predecessor associated with the co-mutation. Algorithmically, the
243 co-mutation list and the map can be created while walking from an initial node (any node other
244 than the root), in the direction to the associated root, up to the node whose distance to the initial
245 node is below a certain threshold. The rest of the procedure is as described previously for
246 calculating the supports for single mutations. The complete procedure for calculating supports for
247 co-mutations is formalized in **Algorithm 1**.

248
249 **Algorithm 1:** Pseudocode for calculating supports for co-mutations from sampled phylogenetic trees.

250 -----
251 **Input:** A positive real number d^* and a set of I phylogenetic trees, i.e., $\{T_i = (V_i, E_i) \mid i = 1, 2, \dots, I\}$, where V_i and E_i
252 are the set of nodes and edges in the tree, respectively. The root of the i -th tree is denoted as r_i and each node v in the
253 tree is labelled with the distance of the node to its respective root and the set of mutations observed in the sequence
254 associated with the node, denoted as $d(v, r_i)$ and M_v , respectively.

255
256 **Output:** Function S that maps co-mutations at inferred distances to their support values.

257
258 *# Mapping each co-mutation observed in the phylogenetic trees to the distance of the ancestral (earlier) node*
259 *associated with the co-mutation to its respective root.*

260 **Initialize:** Dictionary **CoM** = {}.

261 **Foreach** $i = 1, 2, \dots, I$ **do:**

262 **Foreach** $v_0 \in V_i - \{r_i\}$ **do:**

263 **Find** a path P from v_0 to r_i .

264 **Foreach** $v \in P - \{r_i\}$ **do:**

```
265         If  $d(v_0, r_i) - d(v, r_i) < d^*$  then:
266             Foreach  $\{m_1, m_2\} \in \{ \{m, n\} | (m, n) \in M_{v_0} \times M_v \cup M_{v_0} \times M_v \}$  do:
267                 If  $\text{CoM}[\{m_1, m_2\}] = \emptyset$  then:
268                      $\text{CoM}[\{m_1, m_2\}] = (d(v, r_i))$ 
269                 Else:
270                     Concatenate  $\text{CoM}[\{m_1, m_2\}]$  and  $(d(v, r_i))$  into
271                      $\text{CoM}[\{m_1, m_2\}]$ .
272
273 # Calculating the supports for co-mutations at inferred distances where the co-mutational signals reaching their peaks
274 Foreach  $\{m_1, m_2\} \in \text{keys}(\text{CoM})$  do:
275     Calculate Gaussian smoothing  $G$  for the array of distance  $\text{CoM}[\{m_1, m_2\}]$ .
276     Find the locations  $d_1, d_2, \dots, d_k$  of the peaks for  $G$  that are local maxima centered in any interval
277     for the distance and their respective height  $h_1, h_2, \dots, h_k$ .
278     Foreach  $i = 1, 2, \dots, k$  do:
279         Calculate support for  $\{m_1, m_2\}$  at distance  $d_i$  using the equations
280          $S(\{m_1, m_2\}, d_i) = |\text{CoM}[\{m_1, m_2\}]| \times h_i / \sum_{j=1}^k h_j$ 
281
```

282 **Identification of significant single-mutations and co-mutations.** The simulated sequence data
283 generated by Pyvolve were under the assumptions of continuous-time Markov model (Markov
284 process), which include the neutrality and site independence. Hence, we could evaluate whether
285 the real sequence data followed the two assumptions by comparing the distribution of relevant
286 statistics calculated from the real sequence data with that calculated from the simulated sequence
287 data. Here we compared the distributions of supports for single-mutations and co-mutations (as
288 described in the previous section) to evaluate the neutrality and site-independency, respectively.
289 Given the site neutrality assumption was rejected, then a certain quantile (e.g., 95% quantile) of
290 the distribution of supports for simulated single-mutations could be used as a threshold for
291 identifying significant single-mutations in the real data. In similar fashion, if the site independence
292 assumption was rejected, then a certain quantile of the distribution of supports for simulated co-
293 mutations could be used as a threshold for identifying significant co-mutations in the real data.

294
295 **Other analyses.** To optimize the pipeline and assess the robustness of the output, we calculated
296 the overlap coefficient and Kendall rank correlation between the list of top single-mutations/co-
297 mutations output by two different runs of the pipeline. For this, the supports for each unique single-

298 mutation/co-mutation from each run were first summed and then the single-mutations/co-
299 mutations were sorted in descending order according to their aggregated support. Given the top N
300 single-mutations/co-mutations $X_N = (x_1, x_2, \dots, x_N)$ from the first run and $Y_N = (y_1, y_2, \dots, y_N)$
301 from the second run, the overlap coefficient was calculated using the following formula:
302 $\text{overlap}(X_N, Y_N) = |X_N \cap Y_N|/N$.

303
304 For calculating the Kendall rank correlation, we first determined the union of X_N and Y_N , i.e., $X_N \cup$
305 Y_N . Then, we assigned a ranking for each single-mutation/co-mutation in $X_N \cup Y_N$ according to the
306 first run ordering as well as the second run ordering. For all single-mutations/co-mutations that
307 were in $X_N \cup Y_N$ but not in X_N , the first run assigned their ranking to $N + 1$. In the same way, for
308 all single-mutations/co-mutations that were in $X_N \cup Y_N$ but not in Y_N , the second run assigned their
309 ranking to $N + 1$. The two ranking assignments for single-mutations/co-mutations in $X_N \cup Y_N$,
310 each of them was sorted in descending order, were then used to calculate the Kendall rank
311 correlation: $\tau = ((\text{number of concordant pairs}) - (\text{number of discordant pairs})) / (L(L - 1)/2)$,
312 where $L = |X_N \cup Y_N|$ and assuming (q_1, q_2, \dots, q_L) and (r_1, r_2, \dots, r_L) be the sorted ranks by the
313 first run and the second run, respectively, pairs of observations (q_i, r_i) and (q_j, r_j) , where $i < j$,
314 are said to be concordant if $q_i > q_j$ and $r_i > r_j$ and discordant if $q_i > q_j$ and $r_i < r_j$, or if $q_i < q_j$
315 and $r_i > r_j$ (if $q_i = q_j$ and $r_i = r_j$, the pair is neither concordant nor discordant).

316
317 Finally, for the interpretation of the single-mutations and co-mutations output by the pipeline, each
318 amino acid site was mapped to H3 numbering and epitope regions (epitope A, B, C, D and E). The
319 mapping of the sites to epitope regions was based on the mapping provided in [36].

320

321 **Results and Discussions**

322

323 **HA sequences of influenza A/H3N2 and outlier analysis**

324

325 We explored the use of the pipeline to uncover significant single-mutations and co-mutations
326 during the evolution of the A/H3N2 HA. For this, the pipeline first subsetted 7,727 non-redundant
327 from 14,301 A/H3N2 HA sequences available in the local influenza genome datasets (the sequence

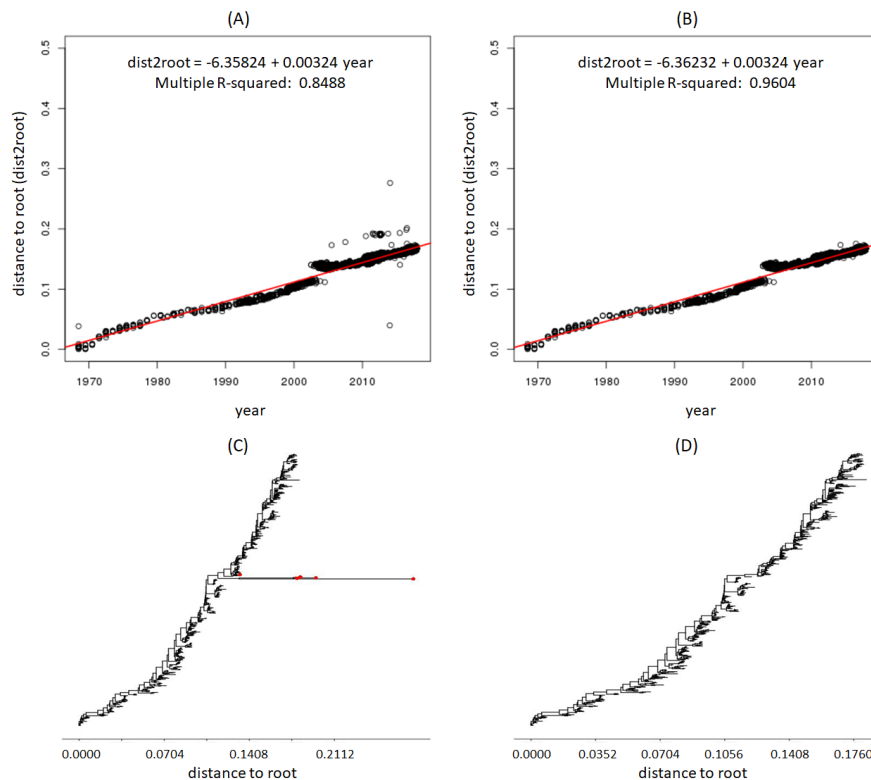
328 metadata are provided in **Table S1**; the acknowledgement table for sequences obtained from
329 GISAID is provided in **Table S2**). An NJ tree was then reconstructed from the aligned sequences
330 and used for checking the assumption of the constant rate of evolution of the HA sequences. As
331 shown in **Fig. 2A**, the assumption was strongly supported by multiple R-squared value of the root-
332 to-tip regression that was >0.95 . Then, using a multiplier for standard deviation of 5 for outlier
333 detection, we identified 58 outliers that were mainly dominated by the sequences collected in the
334 middle of 2012 from a number of regions in North America, including Indiana, Iowa, Michigan
335 Minnesota, Pennsylvania and Ohio. In the phylogenetic tree, the outliers appeared as the tips on
336 the long branch emerging from an internal node at a particular distance to root (**Fig. 2C**; the outliers
337 emerge at distance of 0.11).

338
339 For further analysis, the outliers were removed. The removal of the outliers improved the
340 regression model (**Fig. 2B**), but it did not remove some obvious gap around year 2003-2005 in the
341 scatter plot. Following some investigation, the gap could be linked to the reassortment event and
342 genome-wide selective sweep during the period that replaced the HA of the major circulating
343 influenza A/H3N2 lineage (clade A) with the HA of a minor co-circulating H3N2 lineage (clade
344 B) [37]. The existence of this phenomenon highlights the importance of the phylogenetic tree-
345 based mutational analysis we proposed – sequence alignment-based approaches may lead to
346 misleading list of mutations when analyzing sequence data arise from such phenomenon.

347
348 Despite the gap, we could still safely assume that the substitution rate of the HA of influenza
349 A/H3N2 was constant during the period of sequence data collection due to high R-squared value
350 and its improvement after removing outliers. Indeed, previous studies such as by [38] supported
351 this assumption. Additionally, the assumption that the HA sequences evolve progressively was
352 supported by the ladder-like structure of the phylogenetic tree of HA sequences that excluded the
353 outliers (**Fig. 2D**). Biologically, the ladder-like phylogeny of the HA sequences has been regarded
354 as the consequence of strong directional selection, driven by host immunity [39].

355
356
357
358

359 **Fig. 2.** Root-to-tip regressions and phylogenetic trees of the HA sequences of influenza A/H3N2
360 before and after removing outliers. Outliers are any data point more than five times standard
361 deviation from the average distances of all data points to the regression line. (A) Regression of
362 root-to-tip genetic distance against sampling time for all HA sequences before outlier removal. (B)
363 Regression of root-to-tip genetic distance against sampling time after outlier removal. (C)
364 Neighbor joining tree of a subset of sequences that contain some outliers. The tips corresponding
365 to the outliers are in red. (D) Neighbor joining tree of the same subset of sequences but the outliers
366 are not included.



367

368

369

370 Estimation of evolutionary parameters and simulation of sequence evolution

371

372 Following the outlier analysis, we reconstructed an ML tree under *GTR + G + I* substitution model
373 using the alignment of all sequence data except the outliers. For *GTR + G + I* substitution model,
374 the estimated discrete gamma model parameters were 4 for the number of rate categories and
375 1.1003 for the shape parameters; the estimated proportion of invariant sites was 0.2500; the

376 estimated equilibrium base frequency parameters were 0.4061, 0.1688, 0.1842 and 0.2409 for
377 nucleotide A, C, G and T, respectively; and the estimated rate matrix as follows:

$$378 \quad Q = \begin{bmatrix} 0.0000 & 1.3128 & 6.6816 & 0.4432 \\ 1.3128 & 0.0000 & 0.1288 & 7.5154 \\ 6.6816 & 0.1288 & 0.0000 & 1.0000 \\ 0.4432 & 7.5154 & 1.0000 & 0.0000 \end{bmatrix}$$

379 The estimated $GTR + G + I$ substitution model parameters, along with the structure of the ML tree
380 (that included the length of their branches) and the inferred sequence at the tree root, were used to
381 generated simulated HA sequence dataset under $GTR + G + I$ substitution model (see Methods).

382

383 In addition, we also estimated the substitution rate and the date of origin of the HA of influenza
384 A/H3N2 sequence. We initially estimated these parameters from the root-to-tip regression that
385 corresponds to the ML tree above, which gave the substitution rate of 0.004618 substitution per
386 year and the date of origin of 1967.34). However, in the downstream analyses, the estimated
387 parameters did not provide reasonable estimated years for the inferred mutations. Thus, we took a
388 different approach, i.e., a bootstrap approach, that averaged the estimated regression parameters
389 calculated from each of the 1000 resampled ML trees reconstructed in the next stage of the
390 pipeline. Using this approach, the estimates for the substitution rate and the date of origin were
391 0.004369 substitution per site per year and 1967.90, respectively. These parameter values were
392 proven to be better for mutational analyses. In addition to estimating the years of inferred
393 mutations, the estimate for the substitution rate was also used to calculated the threshold distance
394 between ancestor and predecessor in the resampled phylogenetic trees (the d^* in **Algorithm 1**) for
395 the identification of co-mutations. In particular, we set the expected number of substitutions per
396 site in one year, i.e., 0.004369 substitutions, as the value for d^* . One reason for using such d^* is
397 due to the fact that influenza epidemics occur yearly and vaccines are updated almost every year
398 by WHO; thus, significant mutational patterns should be observed within 1 year.

399

400 **Parameter optimization for mutational analyses using resampled phylogenetic trees and** 401 **setting the threshold for identifying significant single-mutations and co-mutations**

402

403 Two parameters associated with the reconstruction of resampled trees in **Sub-pipeline 4** were
404 considered to significantly affect the output of the mutational analysis by **Sub-pipeline 5** and thus
405 optimized. The first one was the number of sequences randomly selected from each isolation year

406 group (or in other words, sample size per year group), which effectively determine the size of the
407 resampled phylogenetic trees (i.e., the number of taxa in the resampled phylogenetic trees). The
408 second one was the number of the resampled trees or the number of the resampling iterations. The
409 values to be explored for the first parameter were 5, 10, 15 and 20, while for the second parameter
410 were 300, 700, 1000, 1500 and 2000. The optimal parameters were determined by investigating
411 the robustness of the output, i.e., comparing the top 500 single-mutations/co-mutations (after
412 summing the supports for each unique single-mutation/co-mutation and sorting the single-
413 mutations/co-mutations in descending order according to their aggregated support) that were
414 output by the pipeline using different combination of these two parameters. In particular, we varied
415 one parameter while fixing another, and calculated the overlap coefficient and Kendall rank
416 correlation between two ranking groups output by the runs whose parameters being varied were
417 consecutive.

418

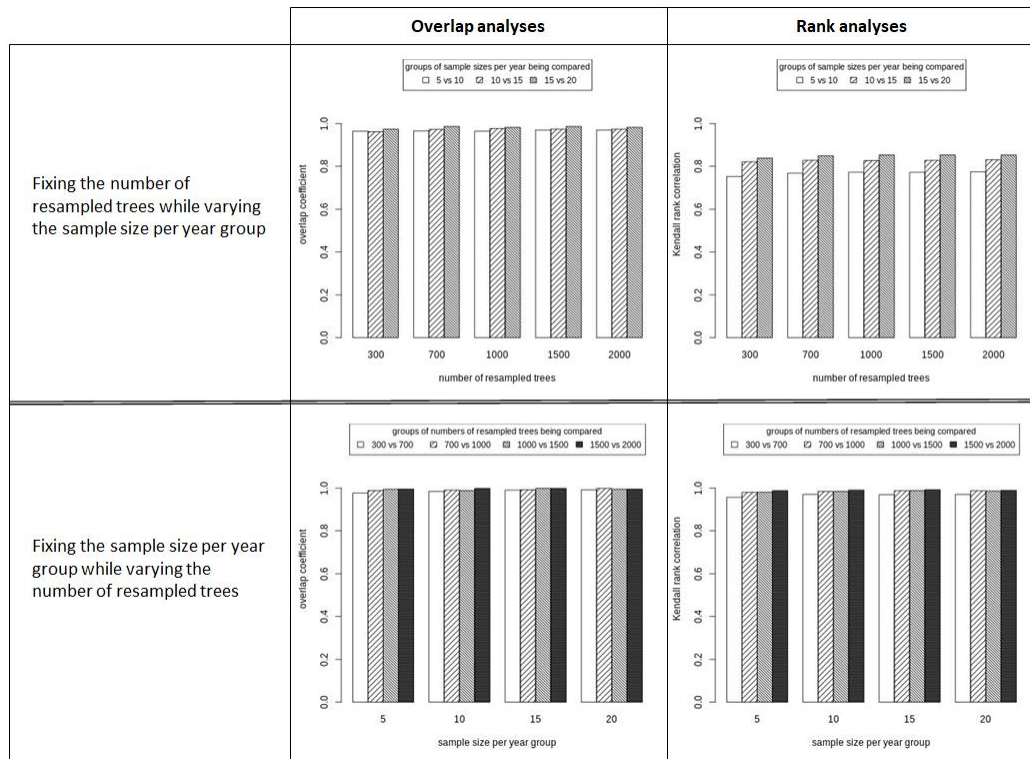
419 As shown in **Fig. 3**, the overlap coefficients between two ranking groups were very high (>.95 and
420 close to 1) for single-mutations regardless we varied the size of the trees or the number of
421 resampled phylogenetic trees. On the other hand, the Kendall rank correlations between two
422 ranking groups stayed high when the moving parameter was the number of resampled trees.
423 However, the correlation got lower when the moving parameter was the sample size per year
424 group; it reached <0.80 when we compared the sample size of 5 and 10. For co-mutations (**Fig. 4**),
425 we once again observed that when the moving parameter was the number of resampled trees, the
426 values for both overlap coefficients and Kendall rank correlations were in general still high
427 (>0.90), except when comparing the number of resampled trees of 300 vs 700 (but still >0.85). But
428 when the moving parameter was the sample size per year group, apparently the overlap coefficients
429 and Kendall rank correlations were higher when we compared the sample size of 10 and 15.
430 Overall, we may conclude that changing the number of resampled trees when it is already >700
431 does not affect the output of the pipeline significantly, and that the sample size per year group
432 between 10 and 15 provides a more consistent result. The same conclusion could be drawn when
433 we lowered the number of top single-/co-mutations to 100 (data not shown).

434

435

436

437 **Fig. 3.** The robustness of single-mutations output by the proposed pipeline when varying the
 438 number of resampled trees and sample size per year group.



439

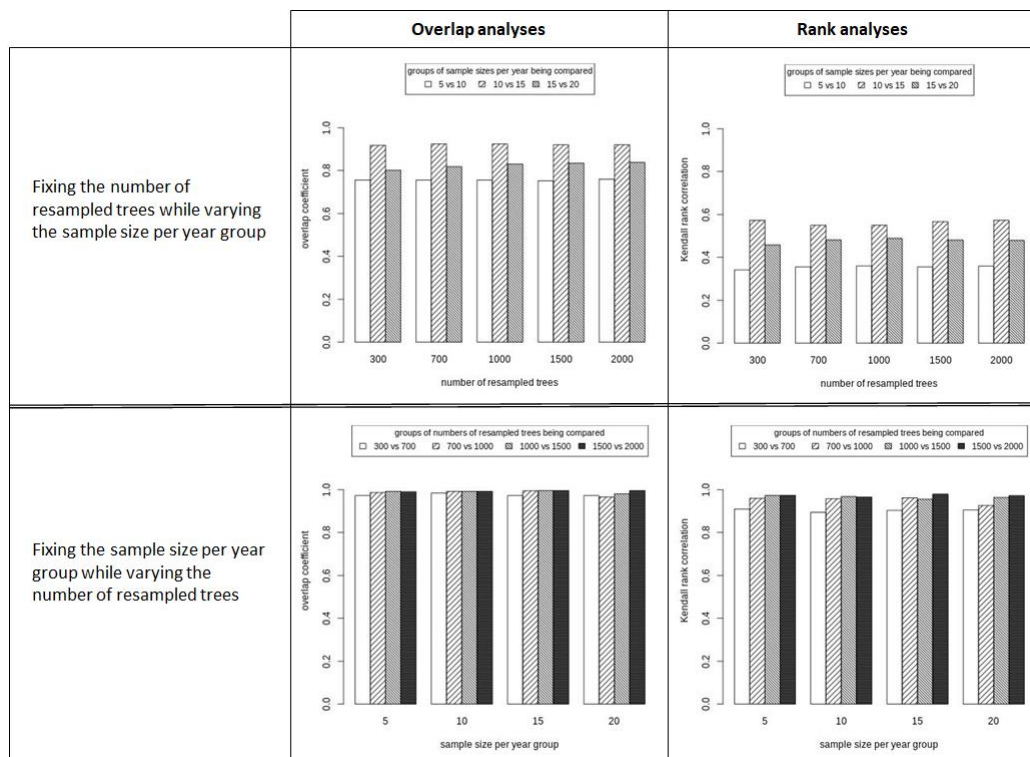
440

441 For further analyses throughout the paper, we fixed the number of resampled trees to 1,000 and
 442 the sample size per year group to 15. To demonstrate that these parameters provided robust output,
 443 the overall pipeline was run 10 times independently. In similar fashion to previous, the overlap
 444 coefficients and Kendall rank correlations between top 500 single-mutations/co-mutations output
 445 by two different runs (note that in total, there were 45 pairs of runs) were calculated to assess the
 446 robustness of the pipeline. But here, the overlap coefficients and Kendall rank correlations were
 447 also calculated for lists of single-mutations/co-mutations that were associated with the simulated
 448 sequence datasets in addition to the real one. As it can be seen in **Fig. 5A** and **5B**, the overlap
 449 coefficients and Kendall rank correlation between two ranking groups in the case of both real and
 450 simulated sequence datasets were very high (>0.90) for single-mutations. For co-mutations, the
 451 overlap coefficients were also still high for both datasets (>0.90); however, the Kendall rank
 452 correlations dropped to about 0.85 and 0.72 for real and simulated datasets, respectively. Of
 453 interest, the overlap coefficients and Kendall rank correlation for real dataset were generally higher
 454 than those for simulated dataset. This result indicates that top single-mutations/co-mutations were

455 highly maintained in the analyses of real dataset, and thus some of them must be at the top not by
 456 chance.

457
 458 In addition to inspecting the overlap coefficient and Kendall rank correlation, we also evaluated
 459 the robustness of the output by examining the QQ plots that compare distributions of supports for
 460 single-mutations/co-mutations from two different runs. If two support distributions are similar,
 461 then the points in the QQ-plots will be mainly scattered on the line $y = x$. As exemplified in **Fig.**
 462 **6A, 6B, 6E** and **6F**, the Q-Q plots indeed suggest that different pipeline runs on the same dataset
 463 (real or simulated one) output distributions of supports for single-mutations/co-mutations that were
 464 highly similar. Thus, the pipeline was robust in term of producing lists of single-mutations/co-
 465 mutations that have particular support distributions.

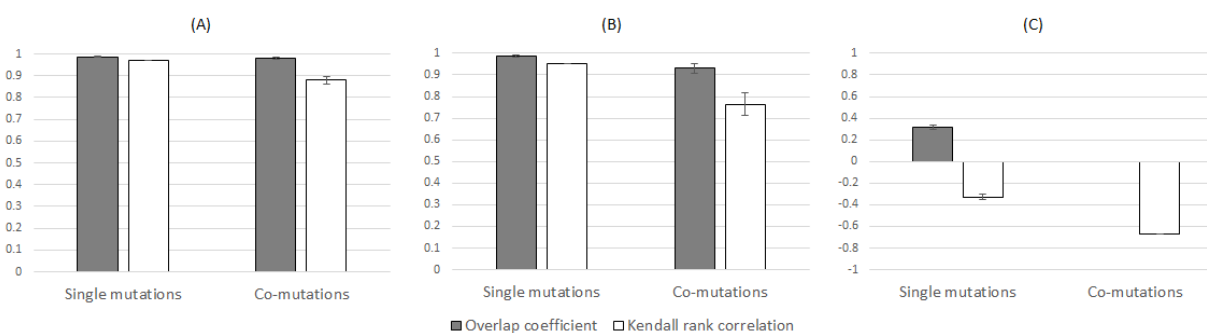
466
 467 **Fig. 4.** The robustness of co-mutations output by the proposed pipeline when varying the number
 468 of resampled trees and sample size per year group.



469
 470
 471 Next, we compared the lists of single-mutations and co-mutations output by **Sub-pipeline 4** and
 472 **Sub-pipeline 5** on different simulated sequence datasets. Expectedly, since different simulations

473 likely produce different mutations, we observed low overlap coefficients (which was even 0 for
474 co-mutation case) and negative Kendall rank correlations (that indicated disagreement) between
475 top 500 single-mutations/co-mutations from different datasets (**Fig. 5C**). But mechanistically,
476 different simulations were expected to produce similar distributions of supports for single-
477 mutations/co-mutations. Indeed, despite data points that deviates from the line $y = x$ in the right
478 tail, this was confirmed by the corresponding QQ-plots (**Fig. 6C** and **6G**).

479
480 **Fig. 5.** Evaluating the robustness of the proposed analysis pipeline on HA proteins sequences of
481 influenza A/H3N2. Averages of overlap coefficients and Kendall rank correlations for all possible
482 pairwise comparisons between the top lists of single-mutations and co-mutations output by 10
483 different runs on (A) real dataset, (B) the same simulated dataset and (C) different simulated
484 datasets. The overlap coefficients and Kendall rank correlations were calculated based on top 500
485 single-mutations or co-mutations of each run.

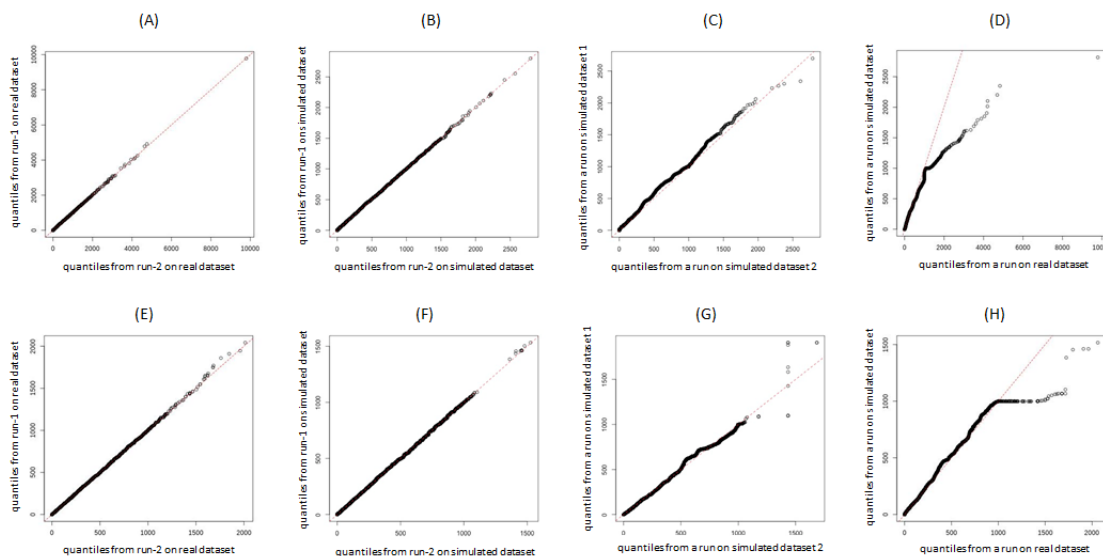


486
487
488 The deviation from the line $y = x$ in the right tail was more obvious when we compared the
489 distributions of supports generated from real and simulated datasets (exemplified in **Fig. 6D** and
490 **6H** for single-mutations and co-mutations, respectively). Overall, this once again indicates that the
491 real dataset contained more extremes (i.e., single-mutations/co-mutations with a high support
492 value) than simulated datasets, which appeared not by chance. Thus, as described in the Methods,
493 we may use the support data given by simulated dataset for the identification of statistically
494 significant single-mutations and co-mutations during the real sequence evolution. For this purpose,
495 we set the 95% quantile of the support distributions for single-mutations from simulated dataset
496 as a threshold for the significance of single-mutations from real dataset for both all path and the
497 longest path analysis, and the 99% quantile for the co-mutation case. The 95% quantile for single-
498 mutations gave a threshold of 999.85 and 1000 for all path and the longest path analyses,

499 respectively, and the 99% quantile for co-mutations gave a threshold of 994. As it can be observed
500 in **Fig. 6D** and **6H**, the threshold for all path's single-mutation and co-mutation analyses were
501 close to the beginning of the deviating points. The appropriateness of choosing higher quantile as
502 a threshold for significant co-mutations was due to higher coverage of co-mutations whose pairs
503 of single-mutations were both significant (94.5% coverage when using 99% quantile, compared to
504 62.9% coverage when using 95% quantile).

505

506 **Fig. 6.** Q-Q plots that compare two distributions of supports for single-mutations and co-mutations
507 output by two different runs on the real dataset (**A** and **E**, respectively), two different runs on the
508 same simulated dataset (**B** and **F**, respectively), two different runs on different simulated datasets
509 (**C** and **G**, respectively), and a run on real dataset versus a run on simulated dataset (**D** and **H**,
510 respectively).



511

512

513

514

515

516

517

518

519

520

521 **Patterns of significant single-mutations during the evolution of the HA of influenza A/H3N2**
522 **viruses**

523

524 In all path analysis, 346 significant single-mutations during the evolution of the HA of human
525 influenza A/H3N2 were identified. The majority of the mutations, i.e., 73.2% of the total
526 significant single-mutations observed in the trees occurred in the epitope regions of the HA protein.
527 In more details, the number of single-mutations observed in epitope A, B, C, D and E were 60, 60,
528 38, 63, and 32 respectively. Nonetheless, a significant number of single-mutations (93 mutations)
529 was also observed in the non-epitope regions. In the longest path analysis, we identified 117
530 significant single-mutations whose majority (77.8%) occurred in the epitope regions, i.e., 24, 24,
531 10, 18 and 15 significant single-mutations observed in epitope A, B, C, D and E, respectively. The
532 number of significant single-mutations observed in the non-epitope regions for the longest path
533 analysis was 26. Almost all significant single-mutations in the longest path analysis were also
534 observed in all path analysis, i.e., 111 out of 117.

535
536 Sites 144 and 145 in epitope A had the most frequent significant single-mutation occurrences in
537 all path analysis, which were 8 and 11 times, respectively (**Table 1**). Interestingly, the mutations
538 at sites 144 and 145 occurred obvious co-occurrences despite their very close proximity in the HA
539 structure (**Fig.7A**). Sites 45 in epitope C and 193 in epitope B followed the list with the number of
540 significant single-mutation occurrences of 7 times. Nonetheless, only 4 mutations at site 144, 3
541 mutations at site 145, 1 mutation at site 193 and none at site 45 were identified in the longest path
542 analysis (**Fig.7B**). On the other hand, 5 significant single-mutations at site 189 in epitope B were
543 all observed in the longest path analysis, and this made site 189 as the top site that had the most
544 frequent significant single-mutation occurrences in the longest path (**Fig. 7A and 7B**). The five
545 significant amino acid substitutions occurring at this position were all different: Q to K (estimated
546 year of occurrence in 1975), K to R (in 1985), R to S (in 1991), S to N (in 2003) and N to K (in
547 2010) (**Fig. 8**), which may indicate the key role of site 189 as a major driver for the evolution of
548 the HA of influenza A/H3N2 viruses.

549

550

551

552 **Table 1.** The most frequent single-mutations during the evolution of the HA of influenza A/H3N2
 553 observed in all path analysis and the longest path analysis.

Location in the resampled trees	Number of occurrences	HA sites						
		Epitope A	Epitope B	Epitope C	Epitope D	Epitope E	Non-epitope	
All path analysis	11	145						
	8	144						
	7		193	45				
	6	124	138	53	173	62		
	5	137, 142	159, 189		219, 226, 229	92	3, 347	
The longest path analysis	5		189					
	4	144						
	3	124, 133, 145	155, 156	50	172, 226	83		

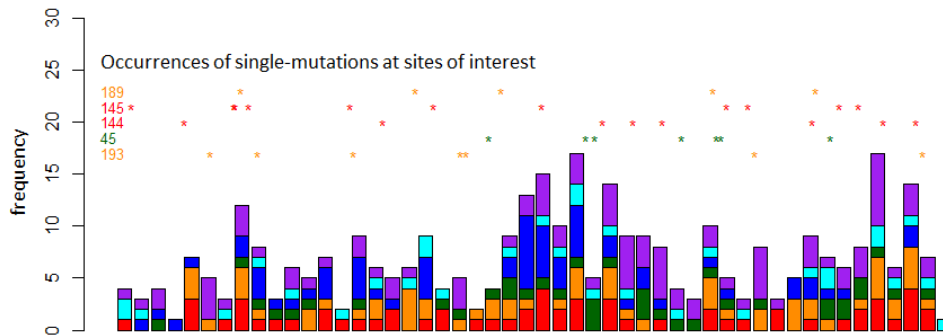
554
 555
 556 The distribution of the significant single-mutation occurrences in all path analysis over the years
 557 from 1968 to 2018 is shown in **Fig. 7A**, and the distribution of the occurrences in the longest path
 558 analysis is shown in **Fig. 7B**. In **Fig. 7A**, we can observe the fluctuation of the number of
 559 significant single-mutation occurrences and a trend in which more mutations tend to be higher in
 560 some ranges of years (e.g., 1991-1995 and 1997-1999) and less in other ranges of years (e.g., 1987-
 561 1989, 2000-2002 and 2004-2008). In **Fig. 7B**, a relatively consistent pattern in the number of
 562 significant single-mutations in the longest path can be observed before around year 2000, where
 563 >3 and ≤ 3 significant single-mutations were alternatively observed across the years. But after
 564 1998, the number was generally ≤ 3 (often 0) over the years except in 2003, when the number
 565 spiked to 11. Considering significant single-mutations occurred over the years in all path analysis,
 566 the absence of significant single-mutations in the longest path analysis is very likely an indication
 567 of the presence of multiple competing lineages. The absence in the period 2000-2002 could be
 568 linked to the presence of multiple competing lineages of clades A, B and C as reported in [40],
 569 while the absence in the recent periods is due to the divergence of clade 3c that began in early
 570 2011 [41]. Furthermore, the fluctuation in the number of significant single-mutations in both all
 571 path and the longest path analyses is relevant with the previous report in [42], which confirmed
 572 alternating periods of stasis (neutral evolution without apparent substantial antigenic change) and
 573 rapid fitness change in the evolution of the HA sequence of influenza A/H3N2.

574

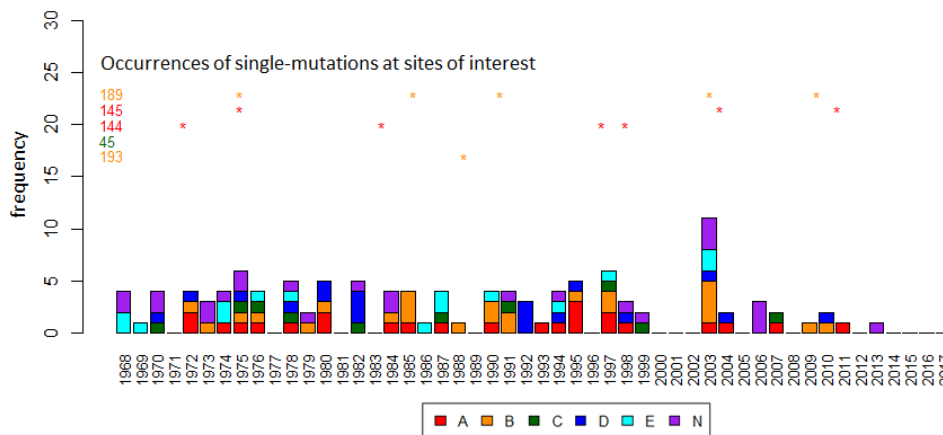
575

576 **Fig. 7.** The yearly frequency of significant single-mutations during the evolution of the HA of
 577 influenza A/H3N2 detected in (A) all path analysis and (B) the longest path analysis. The
 578 occurrences of significant single-mutations at sites of interest are indicated by stars in the
 579 corresponding rows. The contribution of each of epitope regions (A, B, C, D and E) and non-
 580 epitope region (N) to the total yearly frequency are indicated by color (red for epitope A, orange
 581 for epitope B, green for epitope C, blue for epitope D, cyan for epitope E and purple for N).
 582

(A) All path's analysis



(B) The longest path's analysis



583

584

585 To further validate our results, we investigated the overlap between the sites associated with
 586 significant single-mutations in our list and the sites that have been reported to be under selection
 587 pressure in other two studies. First we compared our results against the results by Bush et al. [43]
 588 that were based on analysis of sequences collected between 1983 and 1997, only sites associated
 589 with significant single-mutations that occurred in the period were considered. As a result, we found
 590 that the majority of sites under positive selection pressure in the report were also in our list, i.e.,
 591 23 out of 30 sites. The sites that were captured included sites 121, 124, 133, 135, 137, 138, 142,

592 145, 156, 158, 159, 186, 193, 194, 196, 197, 201, 219, 226, 246, 262, 275 and 276; while the sites
593 that were not captured included sites 80, 128, 182, 190, 220, 310 and 312. In contrast, we recovered
594 only few sites under negative selection pressure in the report, i.e., 3 out of 18 sites. Indeed, these
595 observations were expected since the significant single-mutations we captured were the ones that
596 ought to be fixed in the following generation of HA sequences of the viruses. The coverage of sites
597 under positive selection pressure was further confirmed when comparing our list with the result in
598 [44], which interestingly had a moderate overlap with the result in Bush et al. (only 13 sites in the
599 overlap; 22 sites in [44] are not in [43], and 17 sites in [43] are not in [44]). In particular, our list
600 of significant single-mutations in the period before 2012 (to match with the collection dates of
601 sequences in [44]) covered almost all of the sites in the patches under positive selection pressure
602 uncovered in the study, which include sites 47, 48, 50, 53, 62, 92, 94, 137, 140, 142, 144, 145,
603 156-159, 172-175, 186, 188, 189, 192, 193, 196-199, 220, 229, 275 and 276 (sites 91 and 171 were
604 not covered).

605
606 Next, we also revealed that the majority of single-mutations in the relevant period were associated
607 with antigenic cluster transitions as reported in [11]. As shown in **Fig. 8**, out of 67 single-mutations
608 (4 of them in non-epitope region) in the report, 51 of them were recovered in our analysis: 40 at
609 the longest path (in black and bolded; 15 of them are underlined to indicate that their occurrence
610 was in very close proximity to the year of the new antigenic cluster emergence) and 11 at non-
611 longest paths (in blue and bolded; 1 of them is underlined to indicate that its occurrence was in
612 very close proximity to the year of the new antigenic cluster emergence). In the table, we also
613 showed additional 65 single-mutations that were not in the report.

614
615 Additionally, we also noted that our analysis recovered almost all mutations at the 7 sites near the
616 receptor binding site (i.e., 145, 155, 156, 158, 159, 189 and 193) that had been experimentally
617 shown to be responsible for antigenic cluster transitions during influenza A/H3N2 virus evolution
618 [13]. These include T155Y during transition from HK68 to EN72; Q189K during transition from
619 EN72 to VI75; G158E during transition from VI75 to TX77; K156E during transition from TX77
620 to BA79; Y155H, S159Y and K189R during transition from BA79 to SI87; N145K and N193S
621 during transition from SI87 to BE89; S133D and E156K during transition from SI87 to BE92;
622 N145K during transition from BE92 to WU95; K135T, K156Q and E158K during transition from

623 WU95 to SY97; and Q156H during transition from SY97 to FU02. Only mutation D193N during
 624 transition from VI75 to TX77 was not recovered. Moreover, the significant single-mutations found
 625 in this study also recovered the top 15 cluster-transition determining sites recently reported in [45],
 626 which included sites 122, 133, 135, 144, 145, 155, 156, 158, 189, 190, 193, 197, 262, 276 and 278.
 627

628 **Fig. 8.** Overlap between significant single-mutations and mutations playing a role in antigenic
 629 cluster transitions of influenza A/H3N2 (as reported in [11]). Significant single-mutations obtained
 630 from the longest path analysis are in black; they are bolded if reported in [11] and underlined if
 631 their occurrence is in very close proximity to the year of the new antigenic cluster emergence.
 632 Significant-single mutations only obtained from all path analysis and reported in [11] are in bold
 633 blue; one of them is underlined to indicate that its occurrence was in very close proximity to the
 634 year of the new antigenic cluster emergence. Mutations reported in [11] that are not found in our
 635 analysis is in bold red and underlined. Mutations reported in [11] that are found in our analysis but
 636 their occurrence are not in very close proximity are in bold grey and underlined. (HK: Hong Kong,
 637 EN: England, VI: Victoria, TX: Texas, BA: Bangkok, SI: Sichuan, BE: Beijing, WU: Wuhan, SY:
 638 Sydney, FU: Fujian).
 639

	HK68		EN72		VI75		TX77		BA79				S187	BE89		BE92		WU95		SY97		FU02															
	1968	1970	1972	1974	1976	1978	1980	1982	1984	1986	1988	1990	1992	1994	1996	1998	2000	2002	2004	0.0000	0.0087	0.0175	0.0262	0.0350	0.0437	0.0524	0.0612	0.0699	0.0786	0.0874	0.0961	0.1049	0.1136	0.1223	0.1311	0.1398	0.1485
Epitope A			<u>T122N</u> G144D N137S		<u>N137S</u> S145N T126N	<u>S137Y</u> N137Y N137S	<u>N133S</u> P143S G146S				D144V G124D	<u>G124D</u> T131A N145K	<u>N135K</u> S133D	<u>S135D</u> K145N D124G N145K	<u>N135K</u> K135T	V144I Y137S I144N							<u>A131T</u> A131T	<u>K145N</u>													
Epitope B			<u>T155V</u> N188D		<u>L168Q</u> Q189K S199D	<u>G158E</u> Q164L D193N	<u>K156E</u> T160K Q197R			V163A S159Y Y155H K189R		<u>Y155H</u> K189R N193S	<u>E156K</u> E190D	<u>E156K</u> E190D		<u>V196A</u> K156Q E158K V196A							<u>H155T</u> Q156H	<u>H155T</u> Q156H H155T Q156H S186G S189N													
Epitope C		D275G			<u>N53D</u> I278S	<u>K50R</u> D53N	<u>N53D</u> N54S		K307R			K299R		T276N			<u>N276K</u>	R50G					<u>R50G</u>														
Epitope D		V242I	<u>R207K</u>		<u>R102K</u> F174S I213V I217V I280V	<u>S174F</u> K201R V213I V230I	<u>D172G</u> V217I V244L		N173K I213V N248T					I121T G172D L226I	I226V D172E T121N								S227P V226I														
Epitope E	N63D D81N				D63N T83K	<u>E82K</u> M260I	<u>I62K</u> K82E				E82K K83E			<u>T262N</u> T262N	N262S		<u>K82E</u> R57Q						<u>H75Q</u> E83K	<u>H75Q</u> E83K													
Non-epitope	A(-)3V D31N	E479G R541K	L3F L331I	F3L L(-)2F G(-)1A		D2N I347V			R453K	N2K V384L				K450R	D375N			R452K E386G G225D				<u>L25I</u> V202I W222R G225D	<u>L25I</u> V202I W222R														

640

641

642 Lastly, we present the frequency patterns of amino acid residues during 50 years of evolution of
643 the HA of influenza A/H3N2 viruses at each site associated with significant single-mutations found
644 in our analyses. Given the set of significant single-mutations from all path analysis denoted by A
645 and the set of significant single-mutations from the longest path analysis denoted by B , we grouped
646 the sites into three categories: (1) sites appeared in B but not in $A - B$, (2) sites appeared in $A - B$
647 but not in B , and (3) sites appeared in B and $A - B$. **Fig. 9A** reveals that the hallmark of mutational
648 pattern at sites in the first group was the numerous replacements of a dominant amino acid residue
649 with another dominant amino acid residue, and each dominant amino acids generally could
650 dominate for a long period of time. On the other hand, **Fig. 9B** reveals that sites in the second
651 group often presented temporary appearance of competing amino acid residues. Even though the
652 competing amino acid residue once became the majority, it failed to dominate for a long term.
653 Finally, **Fig. 9C** reveals that sites in the third group presented more dynamics in their mutational
654 patterns, which combined the characteristics mentioned earlier. Practically, with regards to the
655 notions in [11], sites in the first group may play more roles in the enhancement of antigenic drift
656 or shaping the evolution of the HA; sites in the second group may play more roles in compensatory
657 mutations for retaining higher fitness and associated with clades emerged during specific epidemic
658 seasons; and sites found in the third group could both enhance antigenic drift as well as compensate
659 other mutations that enhanced antigenic drift.

660

661

662

663

664

665

666

667

668

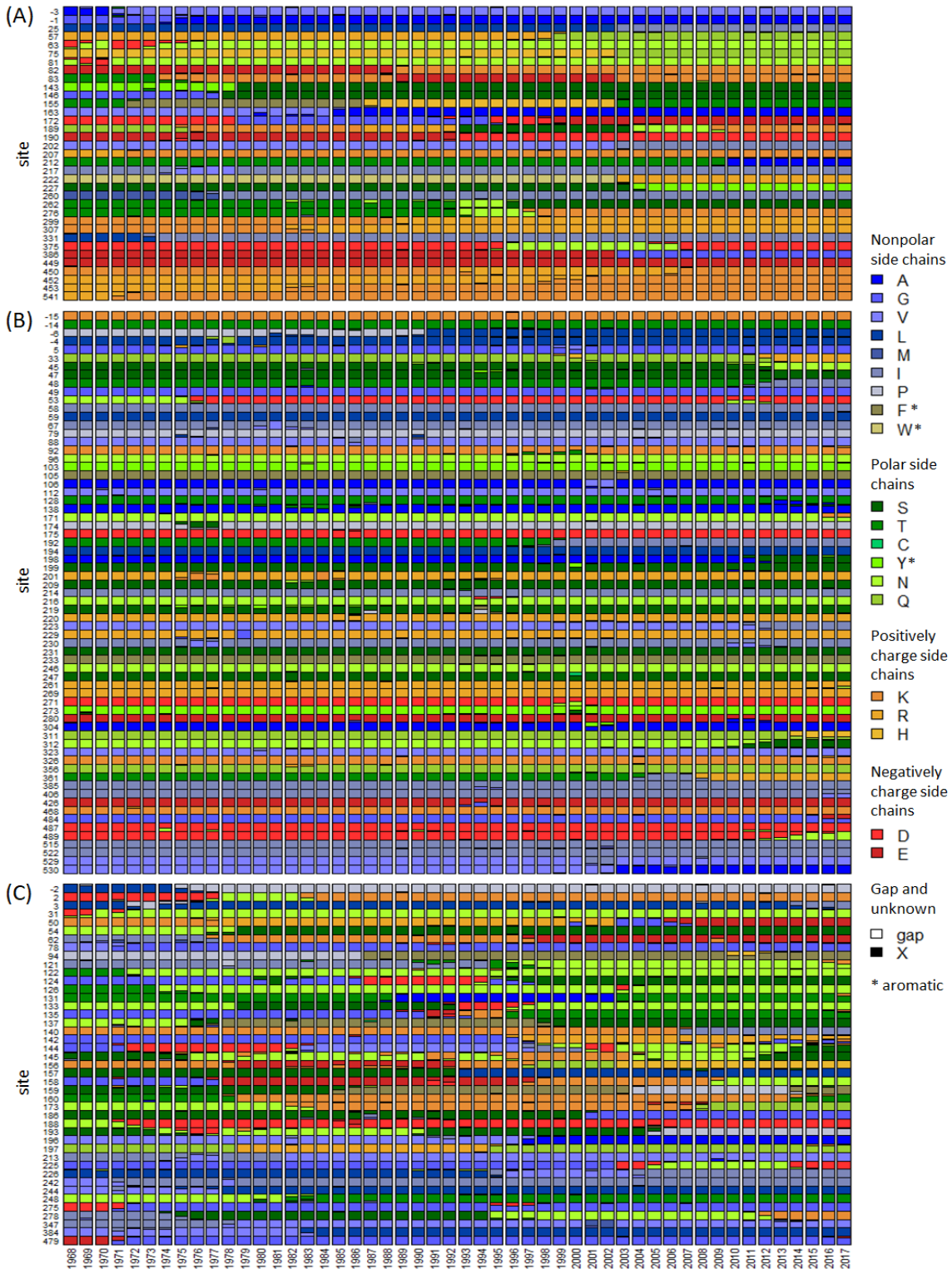
669

670

671

672

673 **Fig. 9.** Yearly frequency of amino acid residues during 50 years of evolution of the HA of influenza
674 A/H3N2 viruses for: (A) sites only found in the longest path analysis, (B) sites only found in all
675 path analysis, and (C) sites found in both all path and the longest path analyses.



677 **Patterns of significant co-mutations during the evolution of the HA of influenza A/H3N2**
678 **viruses**

679
680 Using a threshold distance between ancestor and predecessor in the resampled phylogenetic trees
681 (the d^* in **Algorithm 1**) of 0.004369 substitution per site for co-mutation detection and the 99%
682 quantile of support distribution for co-mutations from the simulated data as a threshold for
683 significance, and only considered co-mutations consisting of a pair of significant single-mutations,
684 we identified 343 significant co-mutations output by the pipeline. However, when considering site
685 pairs of the observed co-mutations, no site pair was observed more than twice during influenza
686 A/H3N2 virus evolution. In fact, we only identified 8 site pairs that occurred twice, including 3-
687 144, 62-144, 62-158, 121-142, 144-158, 155-189, 159-225 and 226-262; the rests occurred only
688 once. Nonetheless, when considering the co-mutational networks, some sites had higher degree or
689 number of co-mutational incidents with other sites. The site with the highest degree was 144, with
690 a degree of 20. Sites 145 and 189 with a degree of 13 followed the top list. Sites 124 and 226 had
691 a degree of 12; sites 92 and 156 had a degree of 11; and the rest had a degree of 10 or less.

692
693 When considering the epitopes, we found that the co-mutations mainly involved sites in non-
694 epitope region (N) and epitope A, B and D. The frequencies for co-mutations involving epitopes
695 A and B and involving N and epitope B were the highest, i.e., 33 times. The frequencies for co-
696 mutations involving N and epitope D, N and epitope A, N and N, epitopes A and D, and epitopes
697 B and D were 28, 27, 27, 23, and 22, respectively; the rests were 20 or less. Next, epitope region
698 with the highest degree was epitope A (104), followed by B (80), D (54), E (26) and C (13). The
699 degree of N was higher than the degree of epitopes C, D and E, i.e., 66. This observation suggests
700 the importance of mutations in non-epitope region that may play a role in maintaining the integrity
701 of the HA.

702
703 Next, we explored the temporal patterns of the significant co-mutations found in this study. For
704 this, we grouped the significant co-mutations by the estimated years of their occurrences by using
705 year group 1968-1972, 1973-1977, 1978-1982, and so on until 2013-2017 (as a note, there was no
706 co-mutation observed in 2018). The networks of co-mutational site pairs observed in each year
707 group and their transitions are shown in **Fig. 10**. The yearly frequency of co-mutations for each

708 year group is also shown on the left or right of the corresponding network. As an initial
709 observation, we can see that the number of co-mutations over the years were continuously up and
710 down. For some years, the number of co-mutations was even very low (less than 5 and even 0),
711 while for some other years, the number was quite high (>10). Then, we can also observe that for
712 some transitions between year groups, the overlap between the sites were relatively small. Only
713 one site was shared by year groups 1973-1977 and 1978-1982, 1983-1987 and 1988-1992, and
714 1998-2002 and 2003-2007; two sites were shared by year groups 2003-2007 and 2008-2012; and
715 three sites were shared by year groups 1968-1972 and 1973-1977. Larger overlaps were observed
716 between year groups 1978-1982 and 1983-1987 (4 overlapping sites), 1988-1992 and 1993-1997
717 (9 sites), 1993-1997 and 1998-2002 (4 sites), and 2008-2012 and 2013-2017 (6 sites). In addition,
718 we can also observe a number of cliques in the co-mutational networks. Of particular interest, we
719 can see that sites with higher degree, i.e., 124, 144, 145, 189 and 226, were usually part of the
720 cliques.

721
722 When considering co-mutations whose pair consisting of significant single-mutations in the
723 longest path analysis, site pairs 137-158 and 155-189 co-mutated twice. Interestingly, sites 83 had
724 the highest degree (13), followed by sites 144 (10), 131 (8), 137 (7), 156 (7) and 189 (7). The co-
725 mutations involving epitopes A and B stayed at the top (16 times), and epitope A still had the
726 highest degree (49). Finally, the corresponding temporal patterns of the significant co-mutations
727 (**Fig. 11**) also revealed the presence of a number of cliques. The lack and absence of the co-
728 mutational networks in the last 2 periods corresponds to the lack and absence of significant single-
729 mutations in the longest path explained previously.

730
731 Overall, consistent with previous report by [42] and [46], our observation suggests that during the
732 evolution of influenza A/H3N2, the increased fitness of the HA was occasionally contributed by
733 simultaneous multi-site co-mutations. Here we argue that the events were likely driven by
734 mutations at a number of influential sites frequently observed as part of cliques in **Fig. 10** and **11**,
735 including sites 83, 144, 145, and 189. Furthermore, we also noted that a new configuration of
736 amino acids at these sites seemed to drive mutations at different sites that were not explored in the
737 previous years.

738

750 **Conclusion**

751

752 In this study, we present a novel phylogenetic tree-based pipeline for analyzing mutational patterns
753 during the evolution of influenza virus sequences. We demonstrated the use of the pipeline to
754 investigate the single-mutational and co-mutational patterns of the HA sequences of influenza
755 A/H3N2 viruses. In addition to known biologically significant mutations in HA and related
756 patterns, our approach allowed the identification of three groups of sites based the outcomes of all
757 path and the longest path analyses on the resampled phylogenetic trees. Sites in each group were
758 shown to exhibit specific characteristics of mutational pattern, which could be linked to their roles
759 in antigenic drift: enhancing antigenic drift, compensating other mutations that enhance antigenic
760 drift, or both. This classification may potentially be useful for evaluating candidate vaccines
761 targeting the HA.

762

763 **Supplementary Material**

764

765 Supplementary data are available at Molecular Biology and Evolution online. The codes for the
766 proposed pipeline are available at DR-NTU (Data) <https://doi.org/10.21979/N9/PDYCUD>.

767

768 **Acknowledgement**

769

770 This project was supported by AcRF Tier 2 grant MOE2014-T2-2-023, Ministry of Education,
771 Singapore and A*STAR-NTU-SUTD AI Partnership Grant.

772

773 **Author Contributions**

774

775 FXI conceived and designed the overall pipeline. FXI, AD and CWL contributed to the writing of
776 python/R/shell codes. FXI wrote the article; XZ helped the writing of the introduction and
777 discussions. JZ and CK reviewed the article.

778

779 References

780

- 781 1. Chen, R. and E.C. Holmes, *Avian influenza virus exhibits rapid evolutionary dynamics*. Mol Biol
782 Evol, 2006. **23**.
- 783 2. Sriwilaijaroen, N. and Y. Suzuki, *Molecular basis of the structure and function of H1*
784 *hemagglutinin of influenza virus*. Proceedings of the Japan Academy, Series B, 2012. **88**(6): p.
785 226-249.
- 786 3. Wilks, S., et al., *A review of influenza haemagglutinin receptor binding as it relates to pandemic*
787 *properties*. Vaccine, 2012. **30**.
- 788 4. Neher, R.A., et al., *Prediction, dynamics, and visualization of antigenic phenotypes of seasonal*
789 *influenza viruses*. Proceedings of the National Academy of Sciences, 2016. **113**(12): p. E1701-
790 E1709.
- 791 5. Codoner, F.M. and M.A. Fares, *Why should we care about molecular coevolution?* Evolutionary
792 Bioinformatics, 2008. **4**: p. 117693430800400003.
- 793 6. Nimrod, G., et al., *In silico identification of functional regions in proteins*. Bioinformatics, 2005.
794 **21**(suppl_1): p. i328-i337.
- 795 7. Martin, L., et al., *Using information theory to search for co-evolving residues in proteins*.
796 Bioinformatics, 2005. **21**(22): p. 4116-4124.
- 797 8. Codoner, F.M., M.A. Fares, and S.F. Elena, *Adaptive covariation between the coat and movement*
798 *proteins of prunus necrotic ringspot virus*. Journal of virology, 2006. **80**(12): p. 5833-5840.
- 799 9. Fares, M.A. and S.A. Travers, *A novel method for detecting intramolecular coevolution: adding a*
800 *further dimension to selective constraints analyses*. Genetics, 2006. **173**(1): p. 9-23.
- 801 10. Kim, Y. and S. Subramaniam, *Locally defined protein phylogenetic profiles reveal previously*
802 *missed protein interactions and functional relationships*. Proteins: Structure, Function, and
803 Bioinformatics, 2006. **62**(4): p. 1115-1124.
- 804 11. Smith, D.J., et al., *Mapping the antigenic and genetic evolution of influenza virus*. Science, 2004.
805 **305**(5682): p. 371-6.
- 806 12. Shih, A.C.-C., et al., *Simultaneous amino acid substitutions at antigenic sites drive influenza A*
807 *hemagglutinin evolution*. Proceedings of the National Academy of Sciences, 2007. **104**(15): p.
808 6283-6288.
- 809 13. Koel, B.F., et al., *Substitutions near the receptor binding site determine major antigenic change*
810 *during influenza virus evolution*. Science, 2013. **342**(6161): p. 976-9.
- 811 14. Quan, L., et al., *Cluster-Transition Determining Sites Underlying the Antigenic Evolution of*
812 *Seasonal Influenza Viruses*. Molecular Biology and Evolution, 2019. **36**(6): p. 1172-1186.
- 813 15. Bush, R.M., et al., *Positive selection on the H3 hemagglutinin gene of human influenza virus A*.
814 *Molecular biology and evolution*, 1999. **16**(11): p. 1457-1465.
- 815 16. Tusche, C., L. Steinbrück, and A.C. McHardy, *Detecting Patches of Protein Sites of Influenza A*
816 *Viruses under Positive Selection*. Molecular Biology and Evolution, 2012. **29**(8): p. 2063-2071.
- 817 17. Blahut, R.E., *Information theory and statistics*. 1987, Addison-Wesley, Reading MA.
- 818 18. Baker, F.N. and A. Porollo, *CoeViz: a web-based tool for coevolution analysis of protein residues*.
819 *BMC bioinformatics*, 2016. **17**(1): p. 119.
- 820 19. Xia, Z., et al., *Using a mutual information-based site transition network to map the genetic*
821 *evolution of influenza A/H3N2 virus*. Bioinformatics, 2009. **25**(18): p. 2309-2317.
- 822 20. Akand, E.H. and K.M. Downard, *Identification of epistatic mutations and insights into the*
823 *evolution of the influenza virus using a mass-based protein phylogenetic approach*. Molecular
824 phylogenetics and evolution, 2018. **121**: p. 132-138.

- 825 21. Chen, H., et al., *Rules of co-occurring mutations characterize the antigenic evolution of human*
826 *influenza A/H3N2, A/H1N1 and B viruses*. BMC Medical Genomics, 2016. **9**(3): p. 229.
- 827 22. Du, X., et al., *Mapping of H3N2 influenza antigenic evolution in China reveals a strategy for*
828 *vaccine strain recommendation*. Nature communications, 2012. **3**: p. 709.
- 829 23. Bao, Y., et al., *The influenza virus resource at the National Center for Biotechnology Information*.
830 J Virol, 2008. **82**(2): p. 596-601.
- 831 24. Shu, Y. and J. McCauley, *GISAID: Global initiative on sharing all influenza data - from vision to*
832 *reality*. Euro Surveill, 2017. **22**(13).
- 833 25. Li, W. and A. Godzik, *Cd-hit: a fast program for clustering and comparing large sets of protein or*
834 *nucleotide sequences*. Bioinformatics, 2006. **22**(13): p. 1658-9.
- 835 26. Edgar, R.C., *MUSCLE: multiple sequence alignment with high accuracy and high throughput*.
836 Nucleic Acids Res, 2004. **32**(5): p. 1792-7.
- 837 27. Kumar, S., G. Stecher, and K. Tamura, *MEGA7: Molecular Evolutionary Genetics Analysis Version*
838 *7.0 for Bigger Datasets*. Mol Biol Evol, 2016. **33**(7): p. 1870-4.
- 839 28. Jukes, T.H. and C.R. Cantor, *Evolution of Protein Molecules*, in *Mammalian Protein Metabolism*,
840 H.N. Munro, Editor. 1969, Academic Press: New York. p. 21-132.
- 841 29. Saitou, N. and M. Nei, *The neighbor-joining method: a new method for reconstructing*
842 *phylogenetic trees*. Mol Biol Evol, 1987. **4**(4): p. 406-25.
- 843 30. Rambaut, A., et al., *Exploring the temporal structure of heterochronous sequences using TempEst*
844 *(formerly Path-O-Gen)*. Virus Evol, 2016. **2**(1): p. vew007.
- 845 31. Schliep, K.P., *phangorn: phylogenetic analysis in R*. Bioinformatics, 2011. **27**(4): p. 592-3.
- 846 32. Tavaré, S., *Some probabilistic and statistical problems in the analysis of DNA sequences*, in
847 *Lectures on Mathematics in the Life Sciences*. 1986. p. 57-86.
- 848 33. Fitch, W.M., *Toward Defining the Course of Evolution: Minimum Change for a Specific Tree*
849 *Topology*. Syst. Zool., 1971. **20**: p. 406-416.
- 850 34. Spielman, S.J. and C.O. Wilke, *Pyvolve: A Flexible Python Module for Simulating Sequences along*
851 *Phylogenies*. PLoS One, 2015. **10**(9): p. e0139047.
- 852 35. Sheather, S.J. and M.C. Jones, *A Reliable Data-Based Bandwidth Selection Method for Kernel*
853 *Density-Estimation*. Journal of the Royal Statistical Society Series B-Methodological, 1991. **53**(3):
854 p. 683-690.
- 855 36. Lee, H.K., et al., *Predicting clinical severity based on substitutions near epitope A of influenza*
856 *A/H3N2*. Infect Genet Evol, 2015. **34**: p. 292-7.
- 857 37. Memoli, M.J., et al., *Recent human influenza A/H3N2 virus evolution driven by novel selection*
858 *factors in addition to antigenic drift*. J Infect Dis, 2009. **200**(8): p. 1232-41.
- 859 38. Hayashida, H., et al., *Evolution of influenza virus genes*. Mol Biol Evol, 1985. **2**(4): p. 289-303.
- 860 39. Volz, E.M., K. Koelle, and T. Bedford, *Viral phylodynamics*. PLoS Comput Biol, 2013. **9**(3): p.
861 e1002947.
- 862 40. Holmes, E.C., et al., *Whole-genome analysis of human influenza A virus reveals multiple*
863 *persistent lineages and reassortment among recent H3N2 viruses*. PLoS Biol, 2005. **3**(9): p. e300.
- 864 41. Gong, Y.N., K.C. Tsao, and G.W. Chen, *Inferring the global phylodynamics of influenza A/H3N2*
865 *viruses in Taiwan*. J Formos Med Assoc, 2019. **118**(1 Pt 1): p. 116-124.
- 866 42. Wolf, Y.I., et al., *Long intervals of stasis punctuated by bursts of positive selection in the seasonal*
867 *evolution of influenza A virus*. Biol Direct, 2006. **1**: p. 34.
- 868 43. Bush, R.M., et al., *Positive selection on the H3 hemagglutinin gene of human influenza virus A*.
869 Mol Biol Evol, 1999. **16**(11): p. 1457-65.
- 870 44. Tusche, C., L. Steinbruck, and A.C. McHardy, *Detecting patches of protein sites of influenza A*
871 *viruses under positive selection*. Mol Biol Evol, 2012. **29**(8): p. 2063-71.

- 872 45. Quan, L., et al., *Cluster-Transition Determining Sites Underlying the Antigenic Evolution of*
873 *Seasonal Influenza Viruses*. *Mol Biol Evol*, 2019. **36**(6): p. 1172-1186.
- 874 46. Shih, A.C., et al., *Simultaneous amino acid substitutions at antigenic sites drive influenza A*
875 *hemagglutinin evolution*. *Proc Natl Acad Sci U S A*, 2007. **104**(15): p. 6283-8.
- 876